

# Supernova Neutrino-Effects on R-Process Nucleosynthesis in Black Hole Formation

T. Sasaqui<sup>1,2,5</sup>, T. Kajino<sup>1,2</sup>, and A. B. Balantekin<sup>3,4</sup>

## ABSTRACT

Very massive stars with mass  $\geq 8M_{\odot}$  culminate their evolution by supernova explosions which are presumed to be the most viable candidates for the astrophysical sites of r-process nucleosynthesis. If the models for the supernova r-process are correct, then nucleosynthesis results could also pose a significant constraint on the remnant of supernova explosions, *i.e.* neutron star or black hole. In the case of very massive core collapse for progenitor mass  $20M_{\odot} \sim 40M_{\odot}$ , a remnant stellar black hole is thought to be formed. Intense neutrino flux from the neutronized core and the neutrinosphere might suddenly cease during the Kelvin-Helmholtz cooling phase because of the black hole formation. It is important and interesting to explore observable consequences of such a neutrino flux truncation. Arguments have recently been given in the literature that even the neutrino mass may be determined from the time delay of deformed neutrino energy spectrum after the cease of neutrino ejection (neutrino cutoff effect).

Here, we study the expected theoretical response of the r-process nucleosynthesis to the neutrino cutoff effect in order to look for another independent signature of this phenomenon. We found a sensitive response of the r-process yield if the neutrino cutoff occurs after the critical time when the expanding materials in the neutrino-driven wind drop out of the Nuclear Statistical Equilibrium (NSE).

---

<sup>1</sup>Department of Astronomy, Graduate School of Science, University of Tokyo, 7-3-1 Hongo, Bunkyo-ku, Tokyo 113-0033, Japan

<sup>2</sup>National Astronomical Observatory and The Graduate University for Advanced Study, 2-21-1 Osawa, Mitaka, Tokyo 181-8588, Japan

<sup>3</sup>Physics Department, University of Wisconsin 1150 University Avenue Madison, WI 53706 U.S.A.

<sup>4</sup>Department of Physics, Tohoku University, Sendai 980-8578, Japan

<sup>5</sup>Present address: Naka Division, Nanotechnology Products Business Group, Hitachi High-Technologies Corporation, 882, Ichige, Hitachinaka, Ibaraki 312-0033, Japan

The r-process nucleosynthesis yields drastically change if the cutoff occurs during the r-process, making maximal effect on the abundance change in  $^{232}\text{Th}$  and  $^{235,238}\text{U}$ . There is large probability of finding this effect in elemental abundances of r-process enhanced metal-deficient halo stars whose chemical composition is presumed to be affected by population III supernovae in the early Galaxy. Using this result, connected with future detection of the time-variation of SN neutrino spectrum, we are able to identify when the black hole formation occurs in the course of SN collapse.

*Subject headings:* supernovae, neutrinos, r-process nucleosynthesis, black holes

## 1. Introduction

In the past eighteen years after SN1987A emerged in the Large Magellanic Cloud, a number of interesting scenarios have been proposed to explain why a pulsar has not been discovered at the supernova (hereafter, SN) remnant. One of the most viable scenarios is the possibility that the pulsation is too weak for emitted X-rays to penetrate through the ambient gas clouds surrounding the SN remnant. Another interesting possibility is that the proto-neutron star (hereafter, NS) was first formed after the core-collapse, emitting thermal neutrinos in twelve seconds during the Kelvin-Helmholtz cooling phase, then became a black hole (hereafter, BH) after deleptonization (Brown & Bethe 1994).

BH formation in core-collapse SNe leads to an interesting theoretical study. If BH formation happens when the flux of neutrinos is still high, abrupt termination within  $\leq 0.5$  ms would emerge as a sharp cutoff of neutrino luminosity at some time after the core bounce. This feature allows celestial model-independent time-of-flight mass tests for the three light neutrino families (Beacom et al. 2001). Beacom et al. (2001) discussed detectable neutrino mass sensitivity that depends strongly on the timing, i.e. how early BH formation occurs after core collapse.

Motivated by these theoretical studies, we consider the possibility that the r-process nucleosynthesis could provide an independent observable signature showing BH formation during high neutrino luminosity epoch. All flavors of neutrinos and antineutrinos from the neutrino-spheres inside the proto-NS are thought to play at least two essential roles in successful SN explosions in “delayed explosion” model. First, successive interactions between intensive flux of neutrinos and materials collapsing into the proto-NS deposit neutrino energy into the ejecta and thus revive the shock propagation leading to a successful breakout through the iron core (Wilson 1985; Bethe & Wilson 1985). Second, in such a neutrino-powered SN

explosion mechanism, the atmosphere of the proto-NS is heated by neutrinos at high entropy  $s/k = 100 - 400$  to form a “hot bubble” flowing out rapidly behind the shock, which is called the neutrino-driven wind. This is a viable candidate site for the r-process (Woosley et al. 1994).

The evolution of the neutrino-driven wind begins from high temperatures about  $10^{10}\text{K}$  at high entropy  $s/k = 100 - 400$ , thus the system is in nuclear statistical equilibrium (NSE) and favors free neutrons, protons, and some amount of  $\alpha$ -particles. As the temperature drops below about  $kT \sim 0.5$  MeV, fast charged particle reactions, which are responsible for interconverting protons into  $\alpha$ -particles and converting  $\alpha$ -particles into composite nuclei, very quickly accumulate “seeds” that have large masses  $70 \leq A \leq 120$  ( $\alpha$ -process). This lasts until the temperature drops to  $kT \sim 0.5/e \sim 0.2$  MeV when the charged particle reactions freeze out ( $\alpha$ -rich freezeout). Below this temperature, only neutron-capture flow goes on, followed by  $\beta$ -decays, and the r-process occurs until the neutrons are exhausted (r-process and freezeout). In Figure 1 we display the evolution of temperature (top panel) and chemical composition of the light elements (bottom panel), indicating the sequence of nuclear reaction processes, *i.e.* the NSE at  $t \leq t_\alpha$ , the  $\alpha$ -process at  $t_\alpha \leq t \leq t_n$ , and the r-process at  $t_n \leq t \leq t_f$ . Here, we define the beginning of the  $\alpha$ -process at  $t = t_\alpha$  when  $kT = 0.5$  MeV, the  $\alpha$ -rich freezeout at  $t = t_n$  when  $kT = 0.5/e \sim 0.2$  MeV, and the r-process freezeout at  $t = t_f$ . We also define the dynamical expansion time of the wind,  $\tau_{dyn}$ , as the e-fold decay time of the temperature from  $kT = 0.5$  MeV (Qian & Woosley 1996), *i.e.*  $\tau_{dyn} = t_\alpha - t_n$ . A short dynamical time can suppress the overproduction of seed nuclei, leaving plenty of free neutrons for the subsequent neutron-capture flow.

The important neutrino reactions during the nucleosynthesis are

$$\nu_e + {}^Z_N A \rightarrow {}^{Z+1}_{N-1} A + e^-, \quad (1)$$

$$\bar{\nu}_e + {}^Z_N A \rightarrow {}^{Z-1}_{N+1} A + e^+, \quad (2)$$

$$\nu_x(\bar{\nu}_x) + {}^Z_N A \rightarrow \left[ \begin{array}{c} {}^{Z-1}_N A + \text{p} \\ {}^Z_{N-1} A + \text{n} \end{array} \right] + \nu'_x(\bar{\nu}'_x), \quad (3)$$

where  $x = \mu, \tau$  are the neutrino flavors, and  ${}^Z_N A$  is the nucleus with proton number  $Z$  and neutron number  $N$ . In particular the charged-current reactions that determine the initial neutron-to-proton ratio are

$$\nu_e + \text{n} \rightarrow \text{p} + e^-, \quad (4)$$

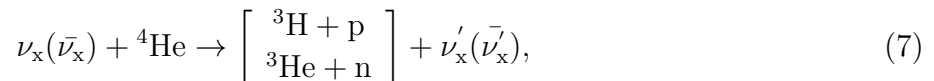
$$\bar{\nu}_e + \text{p} \rightarrow \text{n} + e^+. \quad (5)$$

The neutron-to-proton ratio in the weak equilibrium satisfies (Qian & Woosley 1996),

$$Y_e = \frac{\text{p}}{\text{n} + \text{p}} \approx \left( 1 + \frac{L_{\bar{\nu}_e}}{L_{\nu_e}} \times \frac{\epsilon_{\bar{\nu}_e} - 2\Delta + 1.2\Delta^2/\epsilon_{\bar{\nu}_e}}{\epsilon_{\nu_e} + 2\Delta + 1.2\Delta^2/\epsilon_{\nu_e}} \right), \quad (6)$$

where  $Y_e$  is the electron fraction,  $L_\nu$  is the neutrino luminosity of each species,  $\epsilon_\nu$  is the average energy proportional to  $T_\nu$ , and  $\Delta$  is the mass difference between proton and neutron. In this paper we take  $kT_{\nu_e} = 11.0$  MeV,  $kT_{\bar{\nu}_e} = 19.0$  MeV, and  $kT_{\nu_x, \bar{\nu}_x} = 25.0$  MeV from Woosley et al. (1994) and Qian et al. (1997). Because of the hierarchy of different neutrino flavors  $T_\nu < T_{\bar{\nu}_e} < T_{\nu_x, \bar{\nu}_x}$ , which is the consequence of the different diffusion length scales and the decreasing temperature with increasing radius, this  $Y_e$  value is less than 0.5 when  $L_{\nu_e} = L_{\bar{\nu}_e}$ , as indicated by the numerical simulations of the neutrino transfer (Woosley et al. 1994). Therefore, the whole nucleosynthesis sequence described above and in Figure 1 occurs in the neutron-rich environment with  $Y_e = \frac{p}{n+p} < 0.5$ .

Since the timescale of the  $\alpha$  production is shorter than those of the reactions (4) and (5), protons are locked up into  $\alpha$  particles until they are exhausted. Therefore the reaction (5) does not occur at later times. Thus, the nuclei are neutron rich and the neutrons in the nuclei are degenerate up to higher energy levels than those of the protons. Hence, the reaction (1), which is fundamentally equivalent to the reaction (4), is energetically favorable. In contrast, the reaction (2) can not occur because of the Pauli exclusion principle. Both reactions (1) and (4) have an important role in decreasing the neutron abundance. If the BH is formed and the neutrino luminosity is cut off, neutron abundance is kept high. This may lead to an efficient production of r-process elements because the neutron-to-seed ratio are large under such high neutron abundance conditions (Terasawa et al. 2001). We note that among all neutral-current reactions (3), the spallation of  $\alpha$ -particles;



is most important to accelerate the termination of charged particle reactions during the  $\alpha$ -process by accumulating more seed nuclei and leaving less free neutrons at the end of the  $\alpha$ -process at  $t \approx t_n$  (Meyer 1995). This also strongly affects the r-process nucleosynthesis.

As such, the neutrino cutoff may affect nucleosynthesis because of robust emission of neutrinos before the cutoff time  $t_{cut}$ . Produced r-process abundance pattern may differ from that produced in the SNe leading to the formation of NS. This difference might be important to understand the mechanism of BH formation, which remains an open question.

In our calculations we ignore the effects of neutrino-flavor mixing (Qian and Fuller 1995). Neutrino mixing can significantly alter the r-process nucleosynthesis yields (for a recent discussion see Balantekin and Yuksel (2005)).

This paper will be organized in the following way. In sect. 2, we first review various scenarios of BH formation, and then discuss the conditions under which the neutrino luminosity is cut off in the manner which we will discuss in the present article. In sect. 3, we

describe flow models of neutrino-driven wind in the core-collapse SNe which we adopt in our numerical studies. Several assumptions and approximations are explained. We also explain the nuclear reaction network code in this section. In sect. 5, we show the calculated results on the r-process nucleosynthesis and discuss how different r-element abundances we would obtain, depending on the BH vs. NS formation after the core-collapse. Finally, in sect. 6, we summarize the present paper and discuss the implications of the spectroscopic observations of actinide elements,  $^{232}\text{Th}$  and  $^{235,238}\text{U}$ , in metal-deficient halo stars for testing our results.

## 2. Black Hole Formation and Neutrino Cutoff

We calculate the r-process nucleosynthesis in the SNe where BH is formed. Since we do not know when the BH is formed, we treat the time  $t_{cut}$ , at which the neutrino is cut off, as a parameter. We adopt the constant luminosity,  $L_\nu = 10^{51}\text{ergs}^{-1}$  at  $t \leq t_{cut}$ , and assume that neutrino luminosity is zero after the neutrino cutoff,  $L_\nu = 0$  at  $t_{cut} < t$ . We investigate the dependence of the r-process nucleosynthesis on the value of  $t_{cut}$ .

Stars more massive than  $8M_\odot$  are known to culminate their main sequence lives as core-collapse SNe. In a standard SN explosion where the progenitor star has a mass  $\sim 20M_\odot$ , in general, a NS is formed as a remnant in the center. In heavier progenitor stars, a BH can be formed instead of NS. From a cosmological point of view, the recent discovery of an extremely metal-deficient star suggests that such a supermassive star that induces a BH existed at least in the early universe (Frebel et al. 2005; Iwamoto et al. 2005).

There are so far two different scenarios for BH formation in SN explosions. One of them is a collapsar model. This model is based on a completely different picture from the standard SN. In this model a BH is thought to be formed immediately after a core collapse of SNe. It is phenomenologically possible when the mass of the progenitor star is heavy enough (*e.g.*  $\geq 40M_\odot$ ) to produce a BH. An accretion disk is formed around a BH by pulling materials into the central region and strong X-rays or  $\gamma$ -rays are emitted. This scenario is sometimes invoked to explain  $\gamma$ -ray bursts (MacFadyen & Woosley 1999).

A second scenario is based on a standard core collapse SN explosion. If the proto-NS mass exceeds the maximum NS mass, then a BH can be formed during the SN explosion. Here the maximum mass is thought to be  $2.2M_\odot$  (Beacom et al. 2001; Akmal et al. 1998). This scenario can be useful for the progenitor mass region heavier than that of a standard SN and lighter than that of a collapsar (*e.g.* between  $20M_\odot \sim 40M_\odot$ ). It is the scenario for which the neutrino cutoff effect by the BH formation is obvious, since there can exist a proto-NS *i.e.* neutrino flux from the central neutrino sphere for a short time until a BH is

formed. This situation is different from the collapsar model.

### 3. Flow Models of Neutrino-Driven Wind

#### 3.1. Background

The flow dynamics in non-spherical SN explosion is complicated in the case of collapsars (MacFadyen & Woosley 1999) or hypernovae (Maeda & Nomoto 2003) which are associated with BH formation. The flow in which BH is formed might be different from the standard SN flow leading to a NS formation. We however assume similar models for both flows for the following reasons. The first reason is that in this work we are mainly interested in the consequence of the neutrino-cutoff, i.e. how it destroys neutron richness and affects the final abundance of r-process elements. Since the r-process condition in Type-II SN explosion leaving NS as a remnant has been studied very well (Woosley et al. 1994; Wittl et al. 1994; Otsuki et al. 2000), it is effective to extensively study the r-process in BH formation in similar models by tuning flow parameters of the neutrino-driven wind.

The second reason is that the luminosity stays at high value of  $10^{51} \sim 10^{52} \text{ ergs}^{-1}$  for each neutrino species before the neutrino-cutoff at 1-2 s in either models of BH formation as discussed in the previous section. As we will discuss below, neutrino heating energy is so efficiently deposited in very short period  $\sim 3 \text{ ms}$  (Otsuki et al. 2000) that the hot bubble may form even in the BH formation.

The third reason is that we have not yet obtained a realistic theoretical simulation of a successful SN explosion except for the model of Wilson (1985). It may be more difficult to simulate BH formation which needs at least two dimensional numerical analysis including the effects of general relativity in order to describe both the dynamics of the accretion disk and jet formation as well as the inner core collapse into BH.

For these reasons we use the approximation of the neutrino-driven wind which is suitable for our purpose to study the neutrino-cutoff effects on the r-process nucleosynthesis.

#### 3.2. Steady-State Flow Model

We adopt the spherical steady-state flow model for the neutrino-driven wind (Qian & Woosley 1996; Takahashi & Janka 1997; Otsuki et al. 2000; Wanajo et al. 2001). This flow model is one which leads to a successful r-process. Even though the entropy per baryon is moderately low,  $s/k \approx 100\text{-}300$ , the r-process can occur in this neutrino-driven wind when

the dynamical expansion timescale becomes much shorter than the collision timescale of neutrino-nucleus interactions. For the present application, such hydrodynamic flow can be approximated (Otsuki et al. 2003) by solving the following non-relativistic equations:

$$4\pi r^2 \rho v = \dot{M}, \quad (8)$$

$$\frac{1}{2}v^2 - \frac{GM}{r} + N_A s_{rad} kT = E, \quad (9)$$

$$s_{rad} = \frac{11\pi^2}{45\rho N_A} \left( \frac{kT}{\hbar c} \right)^3, \quad (10)$$

where  $\dot{M}$  is the rate at which matter is ejected by neutrino heating on the surface of the proto-NS. In Eq. (9), the total energy  $E$  is fixed by the boundary condition on the asymptotic temperature,  $T_a$ ;

$$E = N_A s_{rad} k T_a, \quad (11)$$

and we take into account only photons and  $e^\pm$  pairs in the estimate of the entropy per baryon,  $s_{rad}$ , in Eq. (10). For simplicity, in the present work, we utilize an adiabatic, constant-entropy wind rather than computing neutrino heating explicitly (Otsuki et al. 2000). However, we include both charged- and neutral-current interactions between neutrinos and nuclei in the nucleosynthesis. A constant neutrino luminosity  $L_\nu = 10^{51}$  ergs $^{-1}$  for each neutrino species is also adopted. This model has four parameters, which are the NS mass, entropy, boundary temperature, and mass loss rate.

For the purpose of investigating many different flow models, we use the exponential model (Otsuki et al. 2003) which satisfies

$$\tau_{dyn}^{-1} = -\frac{1}{T - T_a} \frac{dT}{dt}, \quad (12)$$

where  $T_a$  is the asymptotic temperature as defined in Eq. (11) so that the solution can be a good approximation to the exact solution of the set of Eqs. (8) - (11). Under the approximate condition that the entropy ( $s = (11\pi^2/45N_A)(T^3/\rho)$ ) is constant, temperature and density are given for a fixed  $\tau_{dyn}$ . Among many different flow models thus solved, we here adopt typical flows with short dynamical explosion time scales,  $\tau_{dyn} \leq 50$  ms, by varying the entropy:  $(\tau_{dyn} [\text{msec}], s/k) = (5, 355), (10, 480), (20, 750), (30, 1050),$  and  $(50, 1680)$ , where we fixed the other parameters. These models produce almost the same final abundance of r-process elements (Sasaqui, Kajino and Mathews 2005) and can well explain the abundance pattern of neutron-capture elements which were detected in one of the most r-process element enhanced metal-deficient halo star CS22892-052 (Snedden et al. 1996).

### 3.3. Neutrino Heating and Cutoff Time

Otsuki et al. (2000) showed that neutrino heating occurs most effectively at  $r \leq 30$  km from the center of the collapsing core. We found in the same flow model analysis that it takes 3 – 4 ms for the material blowing off the surface from proto-NS to reach 30 km. We discussed in sect. 2 that neutrino emission is followed until abruptly terminated by the BH formation with the appearance of apparent horizon in the first scenario. Finite time elapses before BH forms, and the neutrino luminosity is cutoff at 1 – 2 s (Burrows 1988). In the second scenario the cutoff time is delayed about 10 s for the formation of proto-NS, followed by possibly a phase transition of softening the EOS of core matter, and possibly later mass accretion onto BH. Since the neutrino cutoff time 1 – 2 s or 10 s is larger than the heating time scale 3 – 4 ms, we can assume that the hot bubble may form in the neutrino-driven wind of Type-II SNe that form BH as a remnant.

The temperature of all flows of the neutrino-driven wind used in the present study reaches to  $T_9 \approx 9$  at  $t = 3 - 4$  ms. We adopt this temperature as the typical temperature at which neutrino heating is completed. The entropy of the hot bubble formed stays constant after this time. This justifies our assumption of constant entropy during the nucleosynthesis which follows. Our nucleosynthesis calculation starts from this initial temperature, and time zero refers to the time when the hot bubble reaches  $T_9 \approx 9$  as displayed in Figure 1. It is to be noted that the time in this figure and all others we discuss later is not the time after core collapse or core bounce. Flows of the neutrino-driven wind successively blow off until the neutrino luminosity is cutoff at the time  $t = t_{cut}$ .

## 4. Nucleosynthesis Network

For the calculation of the r-process nucleosynthesis, we employ the reaction network used in Sasaqui et al. (2005a,b), which was developed from the original dynamical network code calculations described in Meyer et al. (1992), Woosley et al. (1994), Terasawa et al. (2001), and Otsuki et al. (2003).

The main feature of the network code developed (Sasaqui et al. 2005a,b) is the improvement in the light-mass nuclear reactions. It has already been discussed in literature (Woosley & Hoffman 1992; Meyer et al. 1992; Woosley et al. 1994) that the  $\alpha(\alpha n, \gamma)^9\text{Be}(\alpha, n)^{12}\text{C}$  reaction sequence is particularly important in the earlier stage of the  $\alpha$ -process at high temperature and high density for the production of r-process seed nuclei. Terasawa et al. (2001) suggested that as long as the expansion timescales of the neutrino-driven winds are short,  $\tau_{dyn} \leq 10\text{ms}$ , a successful r-process occurs (Otsuki et al. 2000). Another nuclear



reaction-flow path along the neutron-rich unstable nuclei may play as significant a role as the  $\alpha(\alpha n, \gamma)^9\text{Be}$  reaction does. Sasaqui et al. (2005a,b) found that this is always the case regardless of the flow models of neutrino-powered SN explosions. They quantitatively identified that the  $\alpha(t, \gamma)^7\text{Li}$  reaction and the subsequent  $^7\text{Li}(n, \gamma)^8\text{Li}(\alpha, n)^{11}\text{B}$  reaction are the most critical reactions in addition to  $\alpha(\alpha n, \gamma)^9\text{Be}(\alpha, n)^{12}\text{C}$  that affect strongly the r-process nucleosynthesis particularly of the actinide elements,  $^{232}\text{Th}$  and  $^{235,238}\text{U}$ . They also found that these different nuclear reaction paths merge at  $^{14}\text{C}$ , which is followed by neutron-capture flows on carbon, nitrogen and oxygen isotopes to manifest a new feature of “semi-waiting” point at the neutron-rich isotopes  $^{16}\text{C}$ ,  $^{18}\text{C}$ , and  $^{24}\text{O}$ . This feature of the “semi-waiting” point is the manifestation of a primary r-process so that the SN nucleosynthesis starts from the high entropy conditions on which the NSE favors neutrons, protons, and some amount of  $\alpha$ -particles as an initial composition and thereby the  $\alpha$ -capture, neutron-capture, and  $\beta$ -decay compete with one another in the light-mass neutron-rich nuclei. Sasaqui et al. (2005a,b) updated many nuclear reaction rates on light-mass neutron-rich nuclei with the help of recently accumulated new experimental data obtained by using radioactive nuclear beams (Nakamura et al. 1999; Sasaqui et al. 2005a,b) and references therein.

We also note that we calculate the nucleosynthesis sequence from the NSE,  $\alpha$ -process,  $\alpha$ -rich freeze-out, r-process, and subsequent beta-decay and alpha-decay, as explained in sect. 1 and in Figure 3, in a single network code rather than to split the calculation into two parts as was done in Woosley et al. (1994). This is important for our present study in looking the observable signatures of BH formation in elemental abundances from the r-process nucleosynthesis.

## 5. Result and Discussions

R-process nucleosynthesis in neutrino-driven wind of Type-II SN explosions has been studied by several authors (Woosley et al. 1994; Wittl et al. 1994; Meyer 1995; Qian & Woosley 1996; Otsuki et al. 2000). The following two conditions prove to be important for a successful r-process:

$$\tau_{dyn} \ll \tau_\nu, \quad (13)$$

$$\tau_{dyn} \ll \tau_{\alpha\alpha n}, \quad (14)$$

where  $\tau_\nu \approx 0.201 \times L_{\nu,51}^{-1} \left(\frac{\epsilon_\nu}{\text{MeV}}\right) \left(\frac{r}{100\text{km}}\right)^2 \left(\frac{\langle\sigma_\nu\rangle}{10^{-41}\text{cm}^2}\right)^{-1}\text{s}$  is the neutrino collision time scale (Qian et al. 1997),  $\tau_{\alpha\alpha n} \approx [\rho^2 Y_\alpha^2 Y_n \langle\sigma v_{\alpha\alpha n}\rangle N_A^2]^{-1}$  is the typical nuclear reaction time scale for  $^4\text{He}(\alpha n, \gamma)^9\text{Be}$  which is the slowest one among all charged particle reaction paths,  $L_{\nu,51}$  is the neutrino flux normalized in units of  $10^{51} \text{ ergs}^{-1}$ ,  $\epsilon_\nu$  is the averaged electron-type neutrino

energy  $\sim 11$  MeV,  $r$  is the distance of r-process site from the center of the core,  $\langle\sigma_\nu\rangle$  is the averaged cross section over the neutrino energy spectrum,  $\rho$  is the density of the mass element, and  $N_A$  is Avogadro's number. The former relation (13) describes the condition in which the neutron abundance is kept high when the neutrino process becomes ineffective (see discussion in the introduction), and the latter relation (14) describes the condition in which the neutron-to-seed ratio ( $Y_n/Y_{seed}$ ) is high enough to realize a successful r-process of heavy elements from the seed nuclei.  $Y_{seed}$  is defined as the total seed abundance, i.e.  $Y_{seed} = \sum Y_A$  for  $70 \leq A \leq 120$ .

The time evolution of the temperature  $T_9$ , neutron separation energy  $S_n$ , and neutron and seed abundances  $Y_n$ ,  $Y_{seed}$ , and their ratio  $Y_n/Y_{seed}$  is shown in Figure 1 and Figure 2, separately. Here,  $S_n$  means optimum neutron separation energy. This value is convenient to identify when the classical neutron-capture flow proceeds at low and almost constant value,  $S_n \approx 1$  MeV, and when the freezeout of the n-capture process occurs. Assuming that the transition probabilities for  $(n, \gamma)$  and  $(\gamma, n)$  are equal to each other and nuclear reaction flow stays at a certain nucleus,  $S_n$  is given by

$$S_n = \frac{T_9}{5.040} \{34.075 - \log(Y_n \rho N_A) + \frac{3}{2} \log T_9\}. \quad (15)$$

When  $Y_n$  is large in neutron-rich environment,  $S_n$  is generally small. A drastic increase in  $S_n$  gives us the information on neutron consumption at  $\sim 1$  s as shown in the bottom panel of Figure 1.

The calculated final abundance patterns are shown in Figure 3 for various values of neutrino cutoff time  $t_{cut} = 0.001, 0.005, 0.1$  s, and  $\infty$ . The last case is for no neutrino cutoff. The result is summarized as follows:

(1) When the neutrino cutoff occurs at  $t_{cut} = 0.001$  s under NSE condition (see Figure 1), the influence of the cutoff is largest as neutron abundance  $Y_n$  is kept high (Figure 2) and the r-process becomes effective. This is because the neutrino interactions on neutrons occur for a short time before  $t_{cut}$ . As shown by the dashed line in Figure 3, the heavy r-process elements such as actinides are very effectively produced. However, in this case the cutoff time  $t_{cut} = 1$  ms is too short for shock wave to break out the iron core and SN might fail to explode due to the lack of neutrino heating.

(2) When the neutrino cutoff occurs at  $t_{cut} = 0.005$  s under the condition of efficient  $\alpha$ -process (see Figure 1), the effect of the neutrino cutoff is still large. The dotted line in Figure 3 shows that the r-process proceeds as effectively as in the first case, and the dotted and dashed lines are too close to each other to be separately read out. Both neutron abundance  $Y_n$  and the neutron-to-seed ratio  $Y_n/Y_{seed}$  in Figure 2 are almost the same as those in the first case.

(3) When the neutrino cutoff occurs at  $t_{cut} = 0.1$  s under the condition of efficient neutron-capture process (see Figure 1), the effect of the neutrino cutoff is small, and the final r-process abundance denoted by the dash-dotted line in Figure 3 is very close to the result of no neutrino cutoff (solid line). A notable difference from the previous two cases (1) and (2) is seen in  $Y_n$  and  $Y_n/Y_{seed}$  of Figure 2 for  $t_n < t_{cut}$ .

(4) When we do not take account of the neutrino cutoff for  $t_{cut} = \infty$ , calculated  $^{232}\text{Th}$  abundance is close to the observed lower limit from several metal-deficient halo stars as summarized in Table 3. Both  $Y_n$  and neutron-to-seed ratio  $Y_n/Y_{seed}$  in Figure 2 are close to those of the case (3).

The neutrino cutoff occurring in various nucleosynthesis stages shown in Figure 3 can thus make a remarkable effect on the actinide production. This is an important key feature to identify which SN remnant, BH or SN, forms in the gravitational core-collapse Type-II SN explosions.

We pay special attention to the behavior of the actinides ( $^{232}\text{Th}$ ,  $^{235,238}\text{U}$ ) because of their importance in the cosmochronology. Table 1 and Figure 4 show the ratio of  $^{232}\text{Th}/(^{151}\text{Eu}+^{153}\text{Eu})$ . This is a useful quantity because astronomical observations of metal-deficient halo stars cannot provide each isotopic abundance but just this ratio. We find in Figure 3 that the early cutoff time makes this ratio large. We also find that there appear two outcomes separated by a narrow transitional neutrino cutoff time between 0.01 s and 0.1 s. The “BH outcome” shows a very high abundance ratio which is thought to arise from the events of BH formation, while the “NS outcome” shows a low abundance ratio which may arise from the conditions that do not lead to BH formation. Also, as discussed in sect. 1, the effect of the neutrino cutoff by BH formation is mainly due to the change of neutrons into protons by the weak reaction process (4). So, the drastic change of the final abundance pattern occurs if the neutrino cutoff occurs at a time right after the end of the  $\alpha$ -process and the beginning of the neutron-capture process, i.e.  $t_n \lesssim t$ . This is because drastic environmental change occurs after the  $\alpha$ -rich freezeout of making seed elements at  $t_n \lesssim t$  and only abundant neutrons are easily affected by the weak process (4).

This profile can be fit by the following function.

$$z = z_{t \rightarrow \infty} + \frac{z_1}{1 + (\frac{t}{t_0})^\alpha}, \quad (16)$$

where  $z \equiv ^{232}\text{Th}/(^{151}\text{Eu}+^{153}\text{Eu})$ ,  $t \equiv t_{cut}$ ,  $z_{t \rightarrow \infty}$  means the abundance ratio of no neutrino cutoff,  $z_1 + z_{t \rightarrow \infty} (\equiv z_0)$  means the abundance ratio with no neutrinos,  $t_0$  means the start of the drastic change of the ratio  $z$ , and  $\alpha$  is a constant value. The quantity  $\alpha$  is expected to be model independent and the other quantities are model dependent. In case of Figure 4,

for example,  $z_{t \rightarrow \infty}$  is 0.284,  $z_1$  is 5.20,  $t_0$  is 0.0199 s, and  $\alpha$  is 3.00 (Figure 4) in Otsuki model (Otsuki et al. 2000).

We repeated this calculation using the exponential flow models which are characterized by the different dynamical expansion time scales  $\tau_{dyn} = 5, 10, 20, 30,$  and  $50$  ms, as defined in sect. 3.2. The calculated results are shown in Table 2 and Figure 5 in normalized form of Eq. (16)

$$\xi = \frac{z - z_{t \rightarrow \infty}}{z_1} = \frac{1}{1 + (t/t_0)^\alpha}. \quad (17)$$

Here, we set  $\alpha$ , the parameter which determines the shape of fitting function, to be 3, the same as that of Figure 4. The parameter  $t_0$  in Eq. (16), which corresponds to the time around which a drastic change of the final abundance occurs, is proportional to the dynamical timescale  $\tau_{dyn}$ . In the models with a small dynamical timescale, the temperature drops rapidly and the charged particle reactions are suppressed soon. The freeze out of the  $\alpha$ -process occurs early, so the neutrino cutoff effect leading to a drastic change in the abundance ratio  $z$  occurs early. On the other hand, in the models with a large dynamical timescale, the temperature drops slowly and the charged particle reactions continue to take place. The time of the freezeout of the  $\alpha$ -process becomes later than that in the models with the small dynamical timescale. The drastic change occurs mostly for this reason.

Beacom et al. (2001) proposed that the direct possible signature of BH formation could be the observation of sharp cutoff in the neutrino signal. This may not be a unique good method because there is increasing evidence that the BH formation must be rare at the present epoch for ordinary core-collapse SN scenario, given the low frequency of nearby SNe. Strigari et al. (2003) have shown that direct measurements of the evolution of core-collapse SN rate, which includes the SN rate for BH formation, are consistent with the predictions based on a variety of star formation indicators. From the view point of Galactic chemical evolution, however, different physics may operate (Heger et al. 2003) in the SN explosions in various environments with very different metallicities from the early Galaxy to the present epoch. Neither the neutrino detection studies nor the star formation rate studies can address the possibility that BH formation was a more frequent and dynamically important process in the very early Galaxy of active star formation epoch.

The nucleosynthesis signal proposed in this paper reveals the promising possibility that the effect of neutrino cutoff associated with BH formation would manifest itself in the fossil record of the produced r-process yields. Following remarkable advances in spectroscopic observations, significant information about the abundance of the r-process elements in metal-deficient halo stars has recently been accumulated. These stars are presumed to be second generation stars which were born in the early Galaxy and their elemental abundances were

ideally affected by a few SN episodes of the first generation massive population III stars.

In Figure 3 we show the observed abundance ratios  $^{232}\text{Th}/(^{151}\text{Eu}+^{153}\text{Eu})$  and  $(^{235}\text{U}+^{238}\text{U})/(^{151}\text{Eu}+^{153}\text{Eu})$  of several metal-deficient halo stars tabulated in Table 3. It is interesting that the typical predicted abundances are near the low end of the observed yield in this Figure. This might possibly indicate that those actinides were produced in the first generation SNe associated with remnant NS formation or indicate that only a partial contribution from the SN products associated with BH formation is admixed in the observed r-process elements. The same result is more clearly shown in Figure 4 and 5 which display a band of observed abundance ratios near the “NS outcome” rather than the “BH outcome”.

## 6. Summary and Future Outlook

We investigated the r-process nucleosynthesis in the SNe where BH could form. We found that the r-process abundances could change significantly by neutrino cutoff at the BH formation. This will be one of the predictions about BH formation if metal-deficient halo dwarfs which have such a specific abundance pattern can be found. There appear no observational signatures at the moment indicating that the abundance pattern is made in the events where the BH can be formed. Future observations of more halo stars exhibiting enhanced r-process elements are highly desirable.

We assumed steady state flow of the neutrino-driven wind in our present study. Actually, the flow model must be effected by the BH formation. Therefore reliable models with realistic numerical simulations of general relativistic hydrodynamics are needed. However, the dynamics would be more complex since a very massive star, which evolves to a standard SN, should collapse by accreting materials from the accretion disk and eject part of them in a jet-like explosion. We need to know more details about the dynamics where the BH can be formed. We also need to understand the behavior of the neutrino-driven wind in the environments where the neutrino luminosity is cutoff.

Massive stars associated with BH formation are predicted to occur in the early stage of the Galactic evolution so that they could have ejected nucleosynthesis products which are very different from those ejected from ordinary SNe that leave NS as a remnant. In this article we proposed that actinides could show a remarkable difference for the different neutrino cutoff effects in SNe leaving BH or NS. Similar differences would be found also in the elemental abundances of  $^7\text{Li}$  and  $^{11}\text{B}$  (Yoshida et al. 2004, 2005) which are produced in the neutrino processes in the outer layers of core-collapse SNe. Such productions could impact the Galactic chemical evolution, a point worth investigating. The ultra metal-deficient stars

which have such an abundance pattern might be found in the future using more sophisticated observational techniques.

Table 1: The abundance ratio,  $^{232}\text{Th}/(^{151}\text{Eu}+^{153}\text{Eu})$ , vs. the neutrino cutoff time,  $t_{cut}$  in units of s, in the flow model of the neutrino-driven wind (Otsuki et al. 2000) which is characterized by the dynamical expansion timescale  $\tau_{dyn} = 5$  ms.

cutoff time	$^{232}\text{Th}/(^{151}+^{153}\text{Eu})$
0.0001	5.44
0.0005	5.46
0.0010	5.46
0.0050	5.50
0.0300	1.40
0.0700	0.75
0.1000	0.59
0.2000	0.39
0.3000	0.31
0.5000	0.25
0.7000	0.23
1.0000	0.22
2.0000	0.22
4.0000	0.22
no cutoff	0.22

Table 2: The calculated parameter values,  $z_{t \rightarrow \infty}$ ,  $z_0 (= z_{t \rightarrow \infty} + z_1)$ ,  $t_0$ , and  $\alpha$ , for the fit of the abundance ratio  $z = ^{232}\text{Th}/(^{151}\text{Eu}+^{153}\text{Eu})$  in the functional form of Eq. (16) defined in the text. Five different exponential flow models of the neutrino-driven wind, which are characterized by the dynamical expansion timescales  $\tau_{dyn} = 5, 10, 20, 30$ , and 50 ms, are adopted.

$\tau_{dyn} msec$	$z_{t \rightarrow \infty}$	$z_0$	$t_0$	$\alpha$
	$^{232}\text{Th}/(^{151}\text{Eu}+^{153}\text{Eu})$			
50	0.152	5.68	0.140	3.00
30	0.231	5.90	0.106	3.00
20	0.269	6.43	0.066	3.00
10	0.374	9.31	0.030	3.00
5	0.483	9.00	0.023	3.00

This work has been supported in part by Grants-in-Aid for Scientific Research (13640313, 17540275) and is for Specially Promoted Research (13002001) of the Ministry of Education, Science, Sports and Culture of Japan, and The Mitsubishi Foundation. This work has also been supported in part by the U.S. National Science Foundation Grant No. PHY-0244384 and by the University of Wisconsin Research Committee with funds granted by the Wisconsin Alumni Research Foundation. A.B.B. gratefully acknowledges the 21st Century for Center of Excellence Program “Exploring New Science by Bridging Particle-Matter Hierarchy” at Tohoku University for financial support and thanks the Nuclear Theory Group at Tohoku University for their hospitality.

## REFERENCES

- Akmal, A., Pandharipande, V. R., & Ravenhall, D. G. 1998, *Phys. Rev. C*, 58, 1804
- Balantekin, A.B. and Yuksel, H. 2005 *New J. Phys.* 7, 51
- Burrows, A. 1988, *ApJ*, 334, 891
- Beacom, J. F., Boyd, R. N., & Mezzacappa, A. 2001, *Phys. Rev. D*, 63, 073011
- Bethe, H. A., & Wilson, J. R. 1985, *ApJ*, 295, 14
- Boyd, R. N., et al. 1992, *Physical Review Letters*, 68, 1283
- Brown, G. E., & Bethe, H. A. 1994, *ApJ*, 423, 659
- Christlieb, N., et al. 2004, *A&A*, 428, 1027
- Frebel, A., et al. 2005, *Nature*, 434, 871
- Heger, A., Fryer, C. L., Woosley, S. E., Langer, N., & Hartmann, D. H. 2003, *ApJ*, 591, 288
- Hill, V., et al. 2002, *A&A*, 387, 560
- Honda, S., Aoki, W., Kajino, T., Ando, H., Beers, T. C., Izumiura, H., Sadakane, K., & Takada-Hidai, M. 2004, *ApJ*, 607, 474
- Iwamoto, N., Umeda, H., Tominaga, N., Nomoto, K., & Maeda, K. 2005, *Science Express* 1112997 (astro-ph/0505524 )
- Johnson, J. A., & Bolte, M. 2001, *ApJ*, 554, 888
- MacFadyen, A. I., & Woosley, S. E. 1999, *ApJ*, 524, 262



Table 3: The list of observational data of actinide elemental abundances.  $\log_{\epsilon}(A)$  is equal to  $\log[N(A)/N(H)] + 12$ , where  $N(A)$  is the number abundance of  $A$  and  $N(H)$  is the number abundance of hydrogen. Eu is the total abundances of  $^{151}\text{Eu}$  and  $^{153}\text{Eu}$ , and U is the total abundances of  $^{235}\text{U}$  and  $^{238}\text{U}$ . Observational errors for the data from Honda et al., Westin et al., Sneden et al., Hill et al., Johnson and Bolte, and Christlieb et al. are typically  $\pm 0.15$ ,  $\pm 0.3$ ,  $\pm 0.3$ ,  $\pm 0.07$ ,  $\pm 0.07$  and  $\pm 0.22$ , respectively.

object	$\log_{\epsilon}(\text{Eu})$	$\log_{\epsilon}(\text{Th})$	$\log_{\epsilon}(\text{U})$	Th/Eu	U/Eu	reference
HD6268	-1.56	-1.93		0.69		Honda et al. (2004)
HD110184	-1.91	-2.50		0.55		Honda et al. (2004)
HD115444	-1.97	-1.97		1.00		Honda et al. (2004)
HD186478	-1.34	-1.85		0.60		Honda et al. (2004)
CS30306-132	-1.02	-1.12		0.90		Honda et al. (2004)
CS22892-052	-0.86	-1.42		0.57		Honda et al. (2004)
CS31082-001	-0.59	-0.92		0.72		Honda et al. (2004)
HD115444	-1.63	-2.23		0.55		Westin et al. (2000)
CS22892-052	-0.95	-1.57		0.54		Sneden et al. (2003)
CS31082-001	-0.76	-0.98	-1.92	0.80	0.31	Hill et al. (2002)
HD108577	-1.48	-1.99		0.60		Johnson & Bolte (2001)
HD186478	-1.56	-2.26		0.50		Johnson & Bolte (2001)
HD115444	-1.81	-2.36		0.58		Johnson & Bolte (2001)
BD+8 2856	-1.16	-1.66		0.61		Johnson & Bolte (2001)
M92 VII-18	-1.48	-1.95		0.63		Johnson & Bolte (2001)
M15 K341	-0.88	-1.47		0.55		Sneden et al. (2000)
M15 K462	-0.61	-1.26		0.52		Sneden et al. (2000)
M15 K583	-1.22	-1.70		0.62		Sneden et al. (2000)
CS29497-004	-0.45	-0.96		0.60		Christlieb et al. (2004)

- Maeda, K., & Nomoto, K. 2003, *ApJ*, 598, 1163
- Meyer, B. S. 1995, *ApJ*, 449, L55
- Meyer, B. S., Mathews, G. J., Howard, W. M., Woosley, S. E., & Hoffman, R. D. 1992, *ApJ*, 399, 656
- Mizoi, Y., et al. 2000, *Phys. Rev. C*, 62, 065801
- Nakamura, T. et al. 1999, *Phys. Rev.Lett.* 83, 1112
- Otsuki, K., Tagoshi, H., Kajino, T., & Wanajo, S. 2000, *ApJ*, 533, 424
- Otsuki, K., Mathews, G. J., & Kajino, T. 2003, *New Astronomy*, 8, 767
- Qian, Y.-Z. and Fuller, G.M. 1995, *Phys. Rev. D*, 52, 1479
- Qian, Y.-Z., Haxton, W. C., Langanke, K., & Vogel, P. 1997, *Phys. Rev. C*, 55, 1532
- Qian, Y.-Z. & Woosley, S. E. 1996, *ApJ*, 471, 331
- Sasaqui, T., Kajino, T., Mathews, G. J, Otsuki, K., & Nakamura, T. 2005a, submitted to *ApJ*.(astro-ph/0504526).
- Sasaqui, T., Kajino, T., Mathews, G. J, Otsuki, K., & Nakamura, T. 2005b, *Nucl. Phys. A*, in press.
- Sasaqui, T.and Kajino, T., & Mathews, G. J. 2005, to be submitted to *ApJ*.
- Snedden, C., McWilliam, A., Preston, G. W., Cowan, J. J., Burris, D. L., & Armosky, B. J. 1996, *ApJ*, 467, 819
- Snedden, C., Johnson, J., Kraft, R. P., Smith, G. H., Cowan, J. J., & Bolte, M. S. 2000, *ApJ*, 536, L85
- Snedden, C., et al. 2003, *ApJ*, 591, 936
- Strigari, L. E., Beacom, J. F., Walker, T. P., & Zhang, P. 2005, *Journal of Cosmology and Astro-Particle Physics*, 0504, 017
- Sumiyoshi, K., Utsunomiya, H., Goko, S., & Kajino, T. 2002, *Nuclear Physics A*, 709, 467
- Takahashi, K., & Janka, H.-T. 1997, Origin of matter and evolution of galaxies in the universe '96. Proceedings of an international conference held in Atami, Japan, 18-20 January 1996, Singapore: World Scientific, —c1997, edited by T. Kajino, Y. Yoshii, and S. Kubono, p. 213.

- Terasawa, M., Sumiyoshi, K., Kajino, T., Mathews, G. J., & Tanihata, I. 2001, *ApJ*, 562, 470
- Utsunomiya, H., Yonezawa, Y., Akimune, H., Yamagata, T., Ohta, M., Toyokawa, H., Ohgaki, H., & Sumiyoshi, K. 2001, *Nuclear Physics A*, 688, 340
- Wanajo, S., Kajino, T., Mathews, G. J., & Otsuki, K. 2001, *ApJ*, 554, 578
- Westin, J., Sneden, C., Gustafsson, B., & Cowan, J. J. 2000, *ApJ*, 530, 783
- Wilson, J. R. 1985, *Numerical Astrophysics*, 422
- Witti, J., Janka, H.-T., & Takahashi, K. 1994, *A&A*, 286, 841
- Woosley, S. E., & Hoffman, R. D. 1992, *ApJ*, 395, 202
- Woosley, S. E., Wilson, J. R., Mathews, G. J., Hoffman, R. D., & Meyer, B. S. 1994, *ApJ*, 433, 229
- Yoshida, T., Terasawa, M., Kajino, T., & Sumiyoshi, K. 2004, *ApJ*, 600, 204
- Yoshida, T., Kajino, T., & Hartmann, D. H. 2005, *PRL*, in press (astro-ph/0505043).

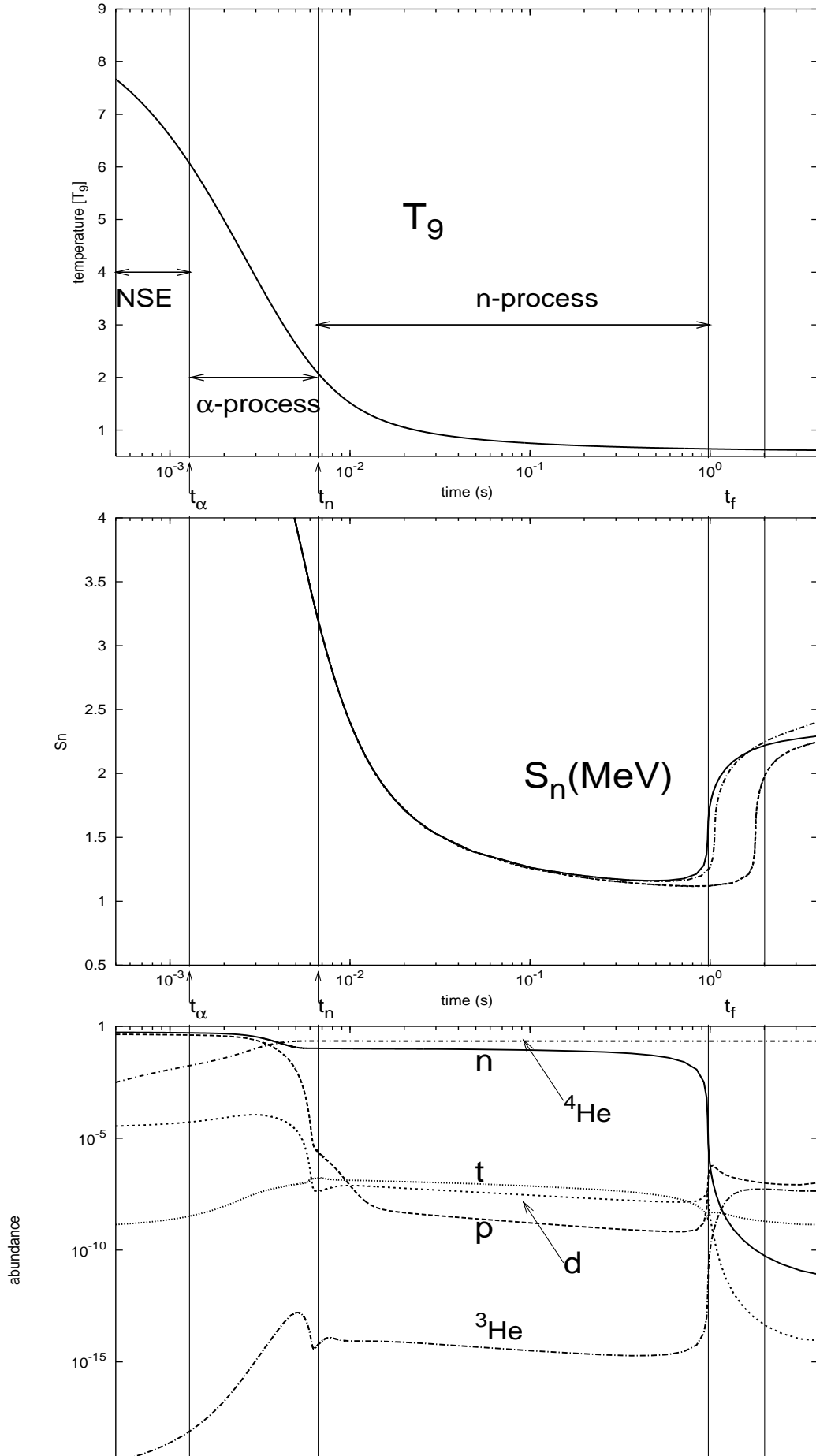


Fig. 1.— Time evolution of temperature  $T_9$  (top panel), neutron-separation energy  $S_n$  [MeV] (middle panel), and abundance of several light elements (bottom panel) in Otsuki flow model (Otsuki et al. 2000). Temperature and light element abundances are for no neutrino cutoff, and neutron-separation energies are for four different neutrino cutoff times 0.001s (dashed line), 0.005 s (dotted line), 0.1 s (dash-dotted line), and  $\infty$  (solid line). Nucleosynthesis starts from NSE, which is taken over by the  $\alpha$ -process during  $t_\alpha \leq t \leq t_n$ , and finally the neutron-capture process proceeds during  $t_n \leq t \leq t_f$  by the time of freezeout of r-process when  $S_n$  drastically increases at  $t_f \sim 1 - 2$  s. See text for more details.

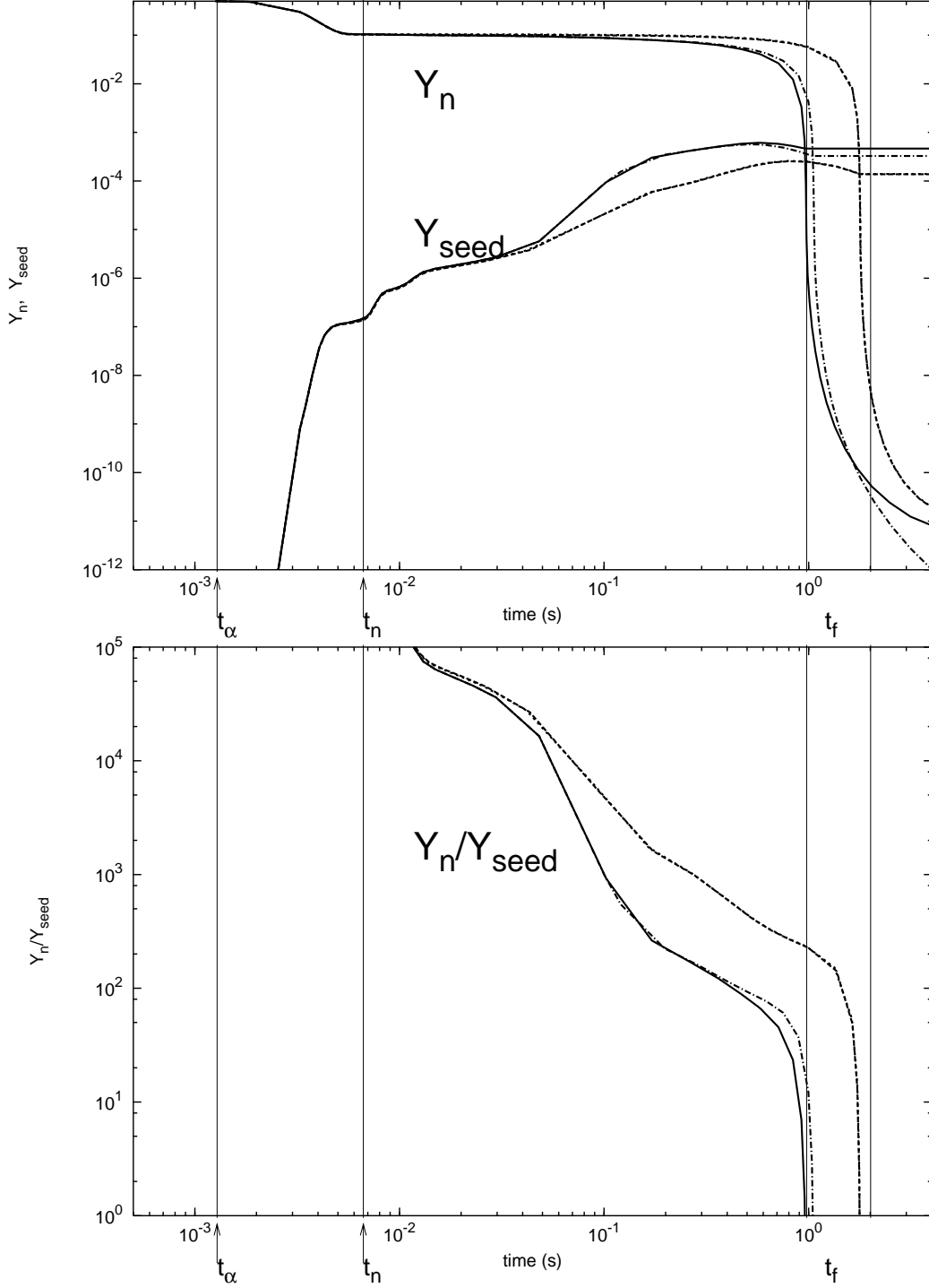


Fig. 2.— Time evolution of neutron abundance  $Y_n$  and seed abundance  $Y_{seed}$  (upper panel), and neutron-to-seed ratio  $Y_n/Y_{seed}$  (lower panel) in Otsuki flow model (Otsuki et al. 2000). The cutoff times are set to be 0.001s (dashed line), 0.005 s (dotted line), 0.1 s (dash-dotted line), and  $\infty$  (solid line), the same as those in Figure 1.

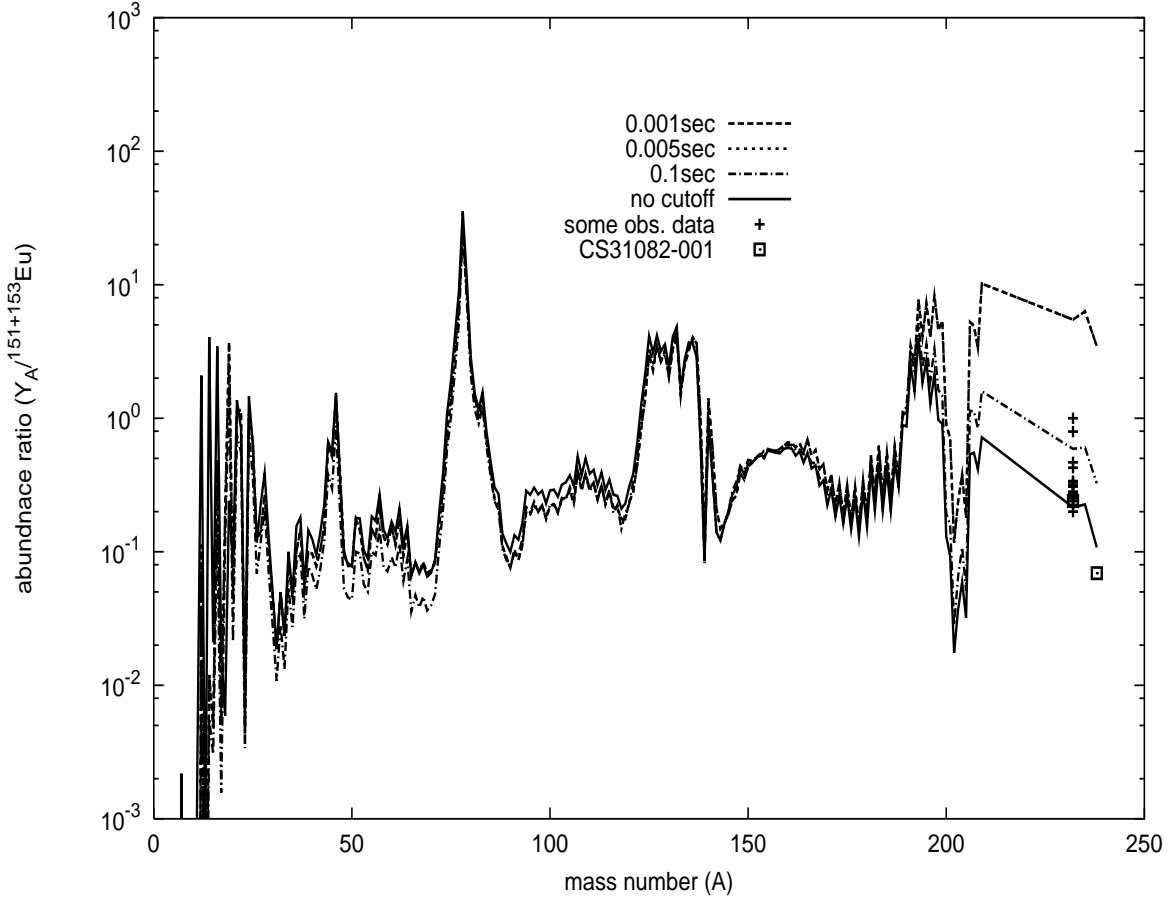


Fig. 3.— Final abundance patterns as a function of mass number in the four cases of different neutrino cutoff times calculated in Otsuki flow model (Otsuki et al. 2000). The cutoff times are set to be 0.001s (dashed line), 0.005 s (dotted line), 0.1 s (dash-dotted line), and  $\infty$  (solid line), the same as those for  $s_n$  in Figure 1. The points indicate recent observational data of abundance ratios  $^{232}\text{Th}/(^{151}\text{Eu}+^{153}\text{Eu})$  and  $(^{235}\text{U}+^{238}\text{U})/(^{151}\text{Eu}+^{153}\text{Eu})$  of metal-deficient halo stars tabulated in Table 3.

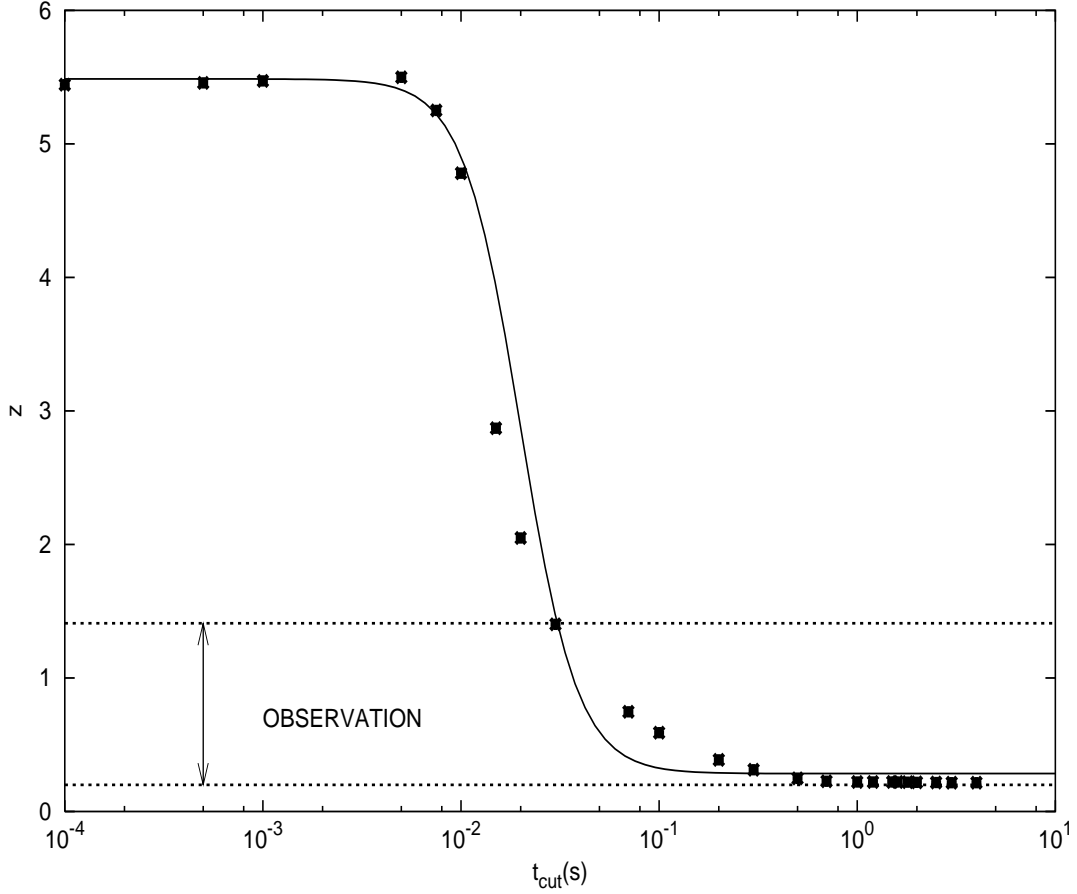


Fig. 4.— Abundance ratio  $z \equiv {}^{232}\text{Th}/({}^{151}\text{Eu}+{}^{153}\text{Eu})$  vs. neutrino cutoff time  $t_{cut}$  calculated in Otsuki flow model (Otsuki et al. 2000). Calculated data points shown in crosses are fit by the solid curve of Eq.(16) with  $\alpha = 3.00$ . The BH outcome (for  $t_{cut} \leq 0.01$ ) and the NS outcome ( $t_{cut} \geq 0.1$ ) appear in two different limits of  $t_{cut}$ . Drastic change occurs when we set the neutrino cutoff time right after the  $\alpha$ -process freezes out and the n-capture process starts. Observed range include both observational errors and dispersion from Table 3. See Table 1 and Figure 5 for more details.



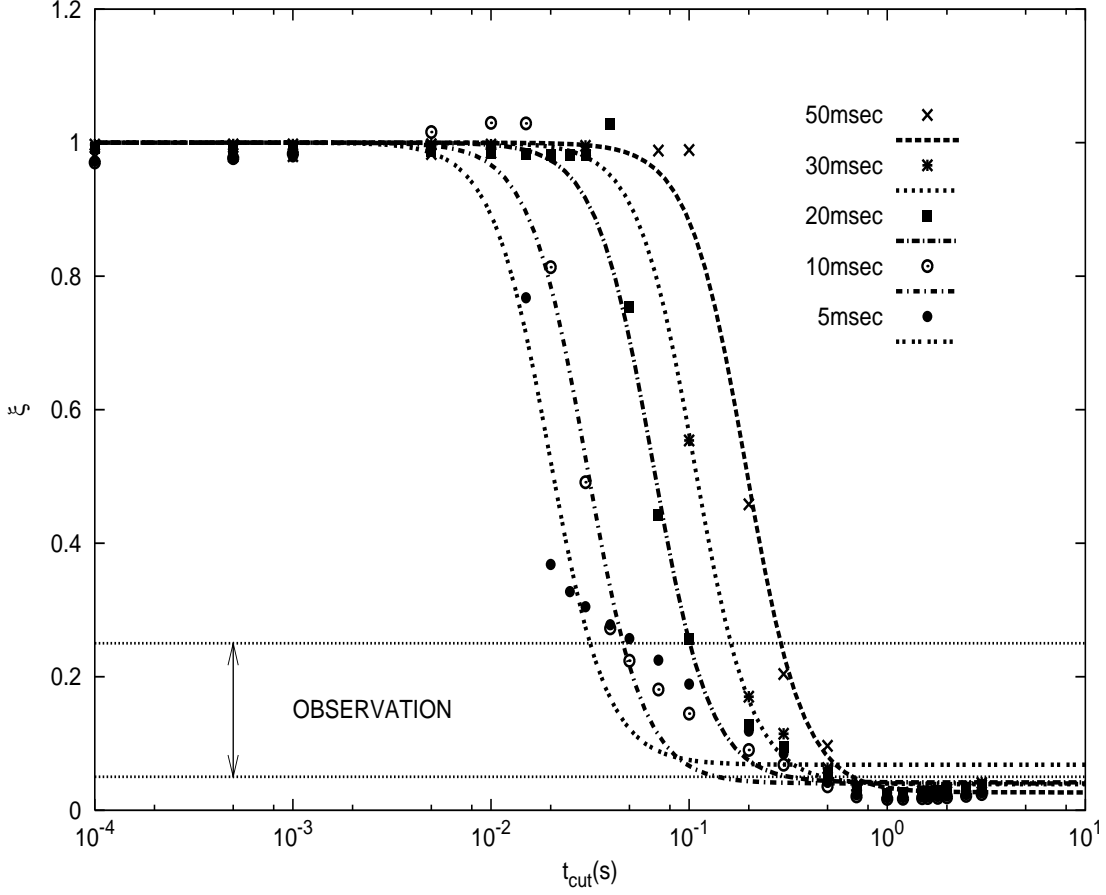


Fig. 5.— Normalized abundance ratio  $\xi = \frac{z - z_{t \rightarrow \infty}}{z_1} = \frac{1}{1 + (t/t_0)^\alpha}$  vs. neutrino cutoff time  $t_{cut}$  calculated in the exponential models which are characterized by the different dynamical expansion time scales  $\tau_{dyn} = 5, 10, 20, 30,$  and  $50$  ms of the neutrino-driven wind, as indicated. Calculated data points are fit by Eq. (17) with various parameter values in Table 2. The parameter  $t_0$ , which corresponds to the time around which a drastic change of the final abundance occurs, is proportional to the dynamical timescale  $\tau_{dyn}$ . Observed range includes both observational errors and dispersion from Table 3. See Table 2 and the text for more details.